Dynamic Characteristics of the Closed Soliton Solution and Phase Analysis of the (3+1)-Dimensional Jimbo-Miwa Equation

M. Asif[1], Harun-Or Roshid[2], M. M. Rahman[3], M. F. Karim[4*], A. Paul[5], Mst. Shekha Khatun[6]

[1,3]Department of Mathematics, Bangladesh University of Engineering and Technology, Dhaka-1000, Bangladesh
[1]Department of Civil Engineering, Dhaka International University, Badda, Satarkul, Dhaka-1212, Bangladesh
[4,5]Department of Mathematical and Physical Science, East West University, Dhaka-1212, Bangladesh
[2,6]Department of Mathematics, Sunamgonj Science and Technology University, Sunamganj-3000, Bangladesh

[*]Corresponding Contact:
Email: fkarim@ewubd.edu

ABSTRACT

The main purpose of this paper is to investigate abundant exact traveling wave solutions (TWSs) of the (3+1)-dimensional Jimbo Miwa model utilizing the innovative auxiliary equation technique. By applying this powerful technique, the obtained solutions reveal and elucidate various types of waves, which are essential for comprehensive studies of complex phenomena such as ocean dynamics and other related scientific and engineering areas. The auxiliary equation method has proven successful in yielding new and analytical soliton solutions, including trigonometric functions, rational functions, hyperbolic functions, and exponential functions for the given model. The results of these solutions are represented using 3-D, contour, and combined 2-D graphs, offering a more detailed and insightful visual interpretation. In particular, the velocity effect becomes more comprehensible when analyzing the 2-D plots. This paper also includes further phase plane analysis of the model to examine the solutions' behavior and characteristics. The results of this investigation have been compared with other researchers' findings available in the literature. This technique proves highly effective for various nonlinear models in generating innovative soliton solutions, which are essential in applied science and engineering.

Key words:
New auxiliary equation approach, (3+1)-dimensional Jimbo Miwa model, Exact Solution, Travelling wave solutions (TWSs)

6/30/2024 **Source of Support:** None, **No Conflict of Interest:** Declared

This article is licensed under a Creative Commons Attribution-NonCommercial 4.0 International License.
Attribution-NonCommercial (CC BY-NC) license lets others remix, tweak, and build upon work non-commercially, and although the new works must also acknowledge & be non-commercial.

INTRODUCTION

Nonlinear evolution equations explain different nonlinear characteristic phenomena in the natural and applied sciences, including fluid mechanics, quantum mechanics, optics, electromagnetism, plasma physics, biomathematics, shallow water waves, oceanography,

mathematical finance, and many others. Nonlinear evolution equations (NLEEs) have various types of solution structures and infinite-dimensional solution spaces, highlighting the challenges associated with determining analytical solutions due to the large dimensions of space variables and the nonlinearity of the differential equations.

In scientific and engineering applications, discovering explicit traveling wave solutions (TWSs) to nonlinear models is crucial as it offers appreciated insights into the workings of the complex phenomena of these equations. The research used scientific techniques to provide reliable solutions for nonlinear equations. Several researchers have investigated NLEEs using different techniques including $\left(\frac{G'}{G}\right)$-expansion technique (Mirzazadeh et al., 2014), $tanh$ function method (Malfliet, 2004), rational function method (Zhang & Ma, 2014), $tanh - coth$ technique (Wazwaz, 2007), $sine$-Gordon expansion method (Baskonus et al., 2019), direct algebraic method (Mirhosseini-Alizamini et al., 2020), modified, extended direct algebraic approach, Hirota bilinear direct technique (Al-Ramadhani, 2024), exp-function method (Ma & Zhu, 2012; Ma et al., 2010), the new auxiliary equation approach (Khater et al., 2018), the planner dynamical system approach (Alshammari et al., 2024; Alaoui et al., 2024), Hirota bilinear method (Ma et al., 2012; Ma, 2022), unified method (Osman et al., 2018), Bäcklund transformation (Lü et al., 2015), modified homogeneous balance methods (Tuffour et al., 2024), Homotopy Perturbation method, Darbox transformation (Ma, 2005), and many more (Arshed et al., 2024; Alshammari et al., 2023; Roshid et al., 2020; Ur Rehman et al., 2024). Using the MAPLE and MATLAB computer software, complex computations can be performed.

Many scholars have examined the following $(3 + 1)$-dimensional Jimbo-Miwa model (Wang & Bilige, 2020; Zhang et al., 2021):

$$u_{xxxy} + 3u_y u_{xx} + 3u_x u_{xy} + 2u_{yt} - 3u_{xz} = 0. \quad (1.1)$$

The solution of the equation explains several interesting events in nonlinear physics. The absence of Painlevé features distinguishes it from the KP equation and originates from the KP hierarchy's second member (Yue et al., 2019). Despite lacking a Kac-Moody-Virasoro loop configuration in an algebra of symmetry of Eq. (1.1), it remains infinite-dimensional (Zhang & Chen, 2017). Mehdipoor & Neirameh (2015) used the sub-equation method and obtained trigonometric, hyperbolic, and rational functions for the $(3 + 1)$-dimensional JME. By employing the simplified Hirota's technique, Wazwaz (2017) investigated numerous soliton solutions of various geometrical configurations for each expanded equation, including $(3 + 1)$-dimensional JMEs. Using the Hirota bilinear approach for the extended (3+1)-dimensional JME, Yue et al. (2019) attained four kinds of waves such as soliton, lumps, breathers, and rogue waves. Liu et al. (2020) have attained a type of periodic wave in the extended $(3 + 1)$-dimensional JME by utilizing bilinear form, Backlund transformation, and Lax pair, collectively referred to as the binary bell polynomial scheme. Also, the sech-function approach is used to generate solitary waves. Zhang et al. (2017) utilized the long wave limit and the Hirota bilinear technique to the $(3 + 1)$-dimensional JME, explicitly focusing on their related interactions and rational and semi-rational solutions. Ma & Lee (2009) explored precise and unambiguous solutions to the $(3 + 1)$-dimensional JME using the logical function transformation technique. Wang et al. (2018) discovered lump wave and monster or abnormal wave solutions for the expanded $(3 + 1)$-dimensional JME by employing bilinear representation and symbolic computation. Zhang et al. (2021) applied the bilinear neural network approach and found dark, bright, and episodic wave solutions for the $(3 + 1)$-dimensional JME.

The new auxiliary equation (NAE) method is a relatively recent approach. It has been observed that the NAE technique is readily applicable to various nonlinear evolution equations (NLEEs), including coupled NLEEs. Moreover, it generates singular solutions involving hyperbolic and trigonometric functions and regular solutions. Due to these advantages, the NAE technique has gained considerable interest among researchers. A review of the literature indicates that the analytical solutions of the $(3+1)$-dimensional Jimbo-Miwa equation have not yet been developed using the NAE approach.

This study examines the soliton solutions, which represent the solutions of a broad class of NLEEs describing a physical system modeled by the $(3+1)$-dimensional Jimbo-Miwa equation using the NAE approach. With the appropriateness and simplicity of this technique, we derive several realistic and generic solutions to the equation. By assigning specific values to arbitrary parameters, various wave solutions are obtained. These solitons are novel and have not been reported in the existing literature. Additionally, we present diagrams of the obtained solutions and discuss their physical significance.

This manuscript is structured as follows. The unfamiliar auxiliary equation method is discussed first, followed by its applications. Phase plane analysis and their geometrical construction are then presented. The results are graphically illustrated, along with their physical interpretations. A comparison is provided with other results available in the literature, and finally, a conclusion is made.

METHODOLOGY

The nonlinear evolution equation is to be considered as the construction form:

$$H\left(u, u_x, u_z, u_y, u_t, u_{xx}, u_{xy}, u_{xz}, u_{xt}, u_{yx}, u_{yy}, u_{yz}, u_{yt}, u_{zz}, u_{tt}, \ \ldots\right) = 0. \tag{2.1}$$

Here, H indicates the nonlinear polynomial function covering the function of wave $u(x, y, z, t)$, and the suffixes denote the partial derivatives concerning x, y, z, and t. Using an appropriate wave profile transformation:

$$u(x, y, z, t) = u(\xi), \qquad \xi = px + qy + rz - \omega t. \tag{2.2}$$

Making use of Eq.(2.2), from Eq. (2.1) we attained ODE as:

$$P(u, u', u'', u''', \ldots) = 0. \tag{2.3}$$

Here $(') = \frac{d}{d\xi}$, $('') = \frac{d^2}{d\xi^2}$, and $(''') = \frac{d^3}{d\xi^3}$. The homogeneous balancing rule, including nonlinear and derivative terms, was used to find the positive integer value. Corresponding to the declared technique, the exact solution $is\ as\ follows$: (2.3)

$$u(\xi) = \sum_{r=0}^{N} k_r a^{rf(\xi)}. \tag{2.4}$$

where $k_r (r = 0, 1, 2, \ldots, N)$ are nonzero constants, and $f(\xi)$ is the solution of first order auxiliary equation

$$f'(\xi) = \frac{1}{ln(a)}\left\{ba^{-f(\xi)} + c + da^{f(\xi)}\right\}. \tag{2.5}$$

We find the positive integer of r by applying the homogeneous balancing rule between the nonlinear term and the maximum order derivative term. To generate a system of algebraic equations, we insert Eqs. (2.4) and (2.5) into Eq. (2.3), equating the coefficient of the power of $a^{rf(\xi)}$, for $r = 0, 1, 2, 3 \ldots.$ from both sides. We calculate the values of $k_r (r =$

$0, 1, 2, 3 \ldots), p, q, r, \omega$ and other variables to solve simultaneous equations. Depending on the values of b, c, and d, various cases arise in the solution of Eq. (2.5), which are stated below:

Case 1: when $c^2 - 4bd < 0$ and $d \neq 0$,

$$a^{f(\xi)} = \frac{-c}{2d} + \frac{\sqrt{4bd-c^2}}{2d} tan\left(\frac{\sqrt{4bd-c^2}}{2}\xi\right).$$

or, $$a^{f(\xi)} = \frac{-c}{2d} - \frac{\sqrt{4bd-c^2}}{2d} cot\left(\frac{\sqrt{4bd-c^2}}{2}\xi\right).$$

Case 2: when $c^2 - 4bd > 0$ and d$\neq$ 0,

$$a^{f(\xi)} = \frac{-c}{2d} - \frac{\sqrt{4bd-c^2}}{2d} \tanh\left(\frac{\sqrt{4bd-c^2}}{2}\xi\right).$$

or, $$a^{f(\xi)} = \frac{-c}{2d} - \frac{\sqrt{4bd-c^2}}{2d} \coth\left(\frac{\sqrt{4bd-c^2}}{2}\xi\right).$$

Case 3: when $c^2 + 4b^2 < 0$, $d \neq 0$ and $d = -b$,

$$a^{f(\xi)} = \frac{c}{2b} - \frac{\sqrt{-c^2-4b^2}}{2b} \tan\left(\frac{\sqrt{-c^2-4b^2}}{2}\xi\right).$$

or, $$a^{f(\xi)} = \frac{c}{2b} + \frac{\sqrt{-c^2-4b^2}}{2b} \cot\left(\frac{\sqrt{-c^2-4b^2}}{2}\xi\right).$$

Case 4: when $c^2 + 4b^2 > 0$, $d \neq 0$ and $d = -b$,

$$a^{f(\xi)} = \frac{c}{2b} + \frac{\sqrt{c^2+4b^2}}{2b} \tanh\left(\frac{\sqrt{c^2+4b^2}}{2}\xi\right).$$

or, $$a^{f(\xi)} = \frac{c}{2b} + \frac{\sqrt{c^2+4b^2}}{2b} \coth\left(\frac{\sqrt{c^2+4b^2}}{2}\xi\right).$$

Case 5: when $c^2 - 4b^2 < 0$ and $d = b$,

$$a^{f(\xi)} = \frac{-c}{2b} - \frac{\sqrt{-c^2+4b^2}}{2b} \tan\left(\frac{\sqrt{-c^2+4b^2}}{2}\xi\right).$$

or, $$a^{f(\xi)} = \frac{-c}{2b} - \frac{\sqrt{-c^2+4b^2}}{2b} \cot\left(\frac{\sqrt{-c^2+4b^2}}{2}\xi\right).$$

Case 6: when $c^2 + 4b^2 > 0$ and $d = b$,

$$a^{f(\xi)} = \frac{-c}{2b} - \frac{\sqrt{c^2-4b^2}}{2b} \tanh\left(\frac{\sqrt{c^2-4b^2}}{2}\xi\right).$$

or, $$a^{f(\xi)} = \frac{-c}{2b} - \frac{\sqrt{c^2-4b^2}}{2b} \coth\left(\frac{\sqrt{c^2-4b^2}}{2}\xi\right).$$

Case 7: when $c^2 = 4bd$, $$a^{f(\xi)} = -\frac{2+c\xi}{2d\xi}.$$

Case 8: when $bd < 0, c = 0$ and $d \neq 0$, $$a^{f(\xi)} = -\sqrt{-\frac{b}{d}} \tanh\left(\sqrt{-bd}\xi\right).$$

or, $$a^{f(\xi)} = -\sqrt{-\frac{b}{d}} \coth\left(\sqrt{-bd}\xi\right).$$

Case 9: when $c = 0$ and $b = -d$, $$a^{f(\xi)} = \frac{1+e^{(-2d\xi)}}{-1+e^{(-2d\xi)}}.$$

Case 10: when $b = d = 0$, $a^{f(\xi)} = \cosh(c\xi) + \sinh(c\xi)$.

Case 11: when $b = c = k$ and d= 0, $a^{f(\xi)} = e^{k\xi} - 1$.

Case 12: when $c = d = \psi$ and $b = 0$, $a^{f(\xi)} = \frac{e^{\psi\xi}}{1-e^{\psi\xi}}$.

Case 13: when $c = (b + d)$, $a^{f(\xi)} = \frac{1-be^{(b-d)\xi}}{1-de^{(b-d)\xi}}$.

Case 14: when $c = -(b + d)$, $a^{f(\xi)} = \frac{b-e^{(b-d)\xi}}{d-e^{(b-d)\xi}}$.

Case 15: when $b = 0$, $a^{f(\xi)} = \frac{ce^{c\xi}}{1-de^{c\xi}}$.

Case 16: when $d = c = b \neq 0$, $a^{f(\xi)} = \frac{1}{2}\left(\sqrt{3}\tan\left(\frac{\sqrt{3}}{2}b\xi\right) - 1\right)$.

Case 17: when $d = c = 0$, $a^{f(\xi)} = b\xi$.

Case 18: when $b = c = 0$, $a^{f(\xi)} = \frac{-1}{d\xi}$.

Case 19: when $d = b$ and $c = 0$, $a^{f(\xi)} = \tan(b\xi)$.

Case 20: when $d = 0$, $a^{f(\xi)} = e^{c\xi} - \frac{k}{\psi}$.

Finally, the wave profile solutions from the Eq. (2.1) are obtained by replacing the values of $k_r(r = 0, 1, 2, \dots), b, c, d$ and $f(\xi)$ into Eq. (2.4).

APPLICATION

This part investigates standard and exact TWSs through the new auxiliary equation technique on the $(3 + 1)$-dimensional JME. We applied an appropriate wave profile transformation:

$$u(x, y, z, t) = u(\xi) \quad \text{where} \quad \xi = px + qy + rz - \omega t. \tag{3.1}$$

Setting Eq.(3.1) into Eq. (1.1), we obtained the ODE form

$$p^3 q u^{iv} + 6p^2 q u'' u' - 2q\omega u'' - 3pru'' = 0. \tag{3.2}$$

After integrating and simplifying, we attained the form

$$p^3 q u''' + 3p^2 q (u')^2 - 2q\omega u' - 3pru' = 0. \tag{3.3}$$

We obtain the positive value of $r\ (= 2)$ using the homogeneous balancing rule between u''' and $(u')^2$. The form of the trial solution for Eq.(3.3) is

$$u(\xi) = k_0 + k_1 a^{f(\xi)} + k_2 a^{2f(\xi)}. \tag{3.4}$$

where k_0, k_1 and k_2 are arbitrary constants such that $k_1 \neq 0$ and $k_2 \neq 0$ simultaneously and $f(\xi)$ is the solution of the nonlinear Eq.(2.5). We insert Eq.(3.4) and Eq.(2.5) and Eq.(3.3), and then set the coefficient of $a^{f(\xi)}$ to zero, which produce simultaneous algebraic equations to obtain the outcomes:

$$\omega = -\frac{p(4p^2qbd - p^2qc^2 + 3r)}{2q}, \ k_0 = k_0, k_1 = -2pd, k_2 = 0.$$

When $c^2 - 4bd < 0$ and $d \neq 0$,

$$u_1 = k_0 - 2pd\left(\frac{-c}{2d} + \frac{\sqrt{4bd-c^2}}{2d}\tan\left(\frac{\sqrt{4bd-c^2}}{2}\xi\right)\right). \quad (3.5)$$

or,

$$u_2 = k_0 - 2pd\left(\frac{-c}{2d} - \frac{\sqrt{4bd-c^2}}{2d}\cot\left(\frac{\sqrt{4bd-c^2}}{2}\xi\right)\right). \quad (3.6)$$

When $c^2 - 4bd > 0$ and d≠ 0,

$$u_3 = k_0 - 2pd\left(\frac{-c}{2d} - \frac{\sqrt{-4bd+c^2}}{2d}\tanh\left(\frac{\sqrt{-4bd+c^2}}{2}\xi\right)\right). \quad (3.7)$$

or,

$$u_4 = k_0 - 2pd\left(\frac{-c}{2d} - \frac{\sqrt{-4bd+c^2}}{2d}\coth\left(\frac{\sqrt{-4bd+c^2}}{2}\xi\right)\right). \quad (3.8)$$

When $c^2 + 4b^2 < 0,\ d \neq 0$ and $d = -b$,

$$u_5 = k_0 + 2pb\left(\frac{c}{2b} - \frac{\sqrt{-4bd-c^2}}{2b}\tan\left(\frac{\sqrt{-4bd-c^2}}{2}\xi\right)\right). \quad (3.9)$$

or,

$$u_6 = k_0 + 2pb\left(\frac{c}{2b} + \frac{\sqrt{-4bd-c^2}}{2b}\cot\left(\frac{\sqrt{-4bd-c^2}}{2}\xi\right)\right). \quad (3.10)$$

When $c^2 + 4b^2 > 0,\ d \neq 0$ and $d = -b$,

$$u_7 = k_0 + 2pb\left(\frac{c}{2b} + \frac{\sqrt{4b^2+c^2}}{2b}\tanh\left(\frac{\sqrt{4b^2+c^2}}{2}\xi\right)\right). \quad (3.11)$$

or,

$$u_8 = k_0 + 2pb\left(\frac{c}{2b} + \frac{\sqrt{4b^2+c^2}}{2b}\coth\left(\frac{\sqrt{4b^2+c^2}}{2}\xi\right)\right). \quad (3.12)$$

When $c^2 - 4b^2 < 0$ and $d = b$,

$$u_9 = k_0 - 2pb\left(-\frac{c}{2b} + \frac{\sqrt{4b^2-c^2}}{2b}\tan\left(\frac{\sqrt{4b^2-c^2}}{2}\xi\right)\right). \quad (3.13)$$

or

$$u_{10} = k_0 - 2pb\left(-\frac{c}{2b} - \frac{\sqrt{4b^2-c^2}}{2b}\cot\left(\frac{\sqrt{4b^2-c^2}}{2}\xi\right)\right). \quad (3.14)$$

When $c^2 + 4b^2 > 0$ and $d = b$,

$$u_{11} = k_0 - 2pb\left(-\frac{c}{2b} - \frac{\sqrt{-4b^2+c^2}}{2b}\tanh\left(\frac{\sqrt{-4b^2+c^2}}{2}\xi\right)\right). \quad (3.15)$$

or

$$u_{12} = k_0 - 2pb\left(-\frac{c}{2b} - \frac{\sqrt{-4b^2+c^2}}{2b}\coth\left(\frac{\sqrt{-4b^2+c^2}}{2}\xi\right)\right). \quad (3.16)$$

When $c^2 = 4bd$,

$$u_{13} = k_0 + \frac{2p\left(\xi\sqrt{bd}+1\right)}{\xi}. \quad (3.17)$$

When $bd < 0, c = 0$ and $d \neq 0$, $\quad u_{14} = k_0 + 2pd\sqrt{-\frac{b}{d}}\tanh\left(\sqrt{-bd}\xi\right). \quad (3.18)$

or,

$$u_{15} = k_0 + 2pd\sqrt{-\frac{b}{d}}\coth\left(\sqrt{-bd}\xi\right). \quad (3.19)$$

When $c = 0$ and $b = -d$,

$$u_{16} = k_0 - \frac{2pd\left(1+e^{(-2d\xi)}\right)}{-1+e^{(-2d\xi)}}. \quad (3.20)$$

When $c = d = \psi$ and $b = 0$,

$$u_{17} = k_0 - \frac{2p\psi e^{\psi\xi}}{1-e^{\psi\xi}}. \quad (3.21)$$

When $c = (b + d)$,

$$u_{18} = k_0 + \frac{2pd\left(1-be^{(b-d)\xi}\right)}{1-de^{(b-d)\xi}}. \quad (3.22)$$

when $c = -(b + d)$

$$u_{19} = k_0 - \frac{2pd\left(b-e^{(b-d)\xi}\right)}{d-e^{(b-d)\xi}}. \quad (3.23)$$

When $b = 0$,

$$u_{20} = k_0 - \frac{2pcde^{c\xi}}{1-de^{c\xi}}. \quad (3.24)$$

When $d = c = b \neq 0$,

$$u_{21} = k_0 - pb\left(\sqrt{3}\tan\left(\frac{\sqrt{3}}{2}b\xi\right) - 1\right). \quad (3.25)$$

When $b = c = 0$,

$$u_{22} = k_0 + \frac{2p}{\xi}. \quad (3.26)$$

When $d = b$ and $c = 0$,

$$u_{23} = k_0 - 2bp\tan(b\xi). \quad (3.27)$$

PHASE PLANE ANALYSIS

Set $u' = v$ then Eq. (3.3) becomes

$$p^3qv'' + 3p^2qv^2 - 2q\omega v - 3prv = 0. \quad (4.1)$$

The model (4.1) can be expressed as follows in the form of a dynamical system

$$\frac{dv}{d\xi} = w$$

$$\frac{dw}{d\xi} = Av + Bv^2 \quad (4.2)$$

Here, $A = \frac{2q\omega+3pr}{p^3q}, B = -\frac{3}{p}$. System (4.2) shown that two equilibrium points such that $O(0,0), P\left(-\frac{A}{B}, 0\right)$, and the Hamiltonian form as follows:

$$H(v,w) = w^2 - AV^2 - \frac{2}{3}Bv^3. \quad (4.3)$$

At the equilibrium point, the Jacobian matrices are determined as follows

Det $J_0 = -A$, det $J_p = A$.

The system has two equilibrium points, and it depends on A.

(i) Case 1: if $A > 0$, then O-saddle and P-center

(ii) Case 2: if $A < 0$, then O-center and P-saddle

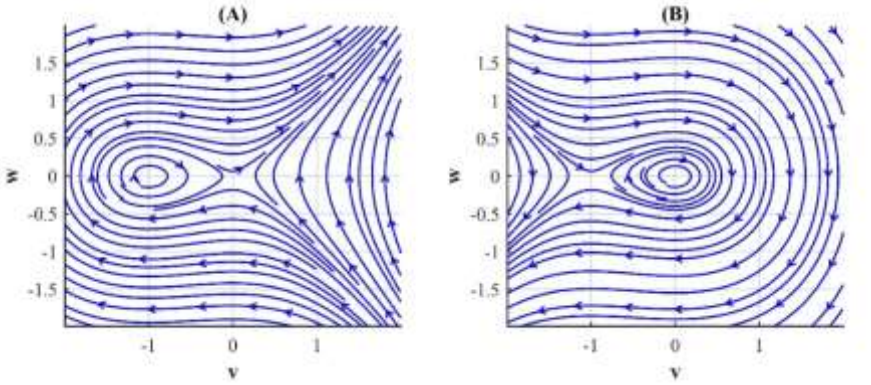

Figure 1 Stream Flows with direction.

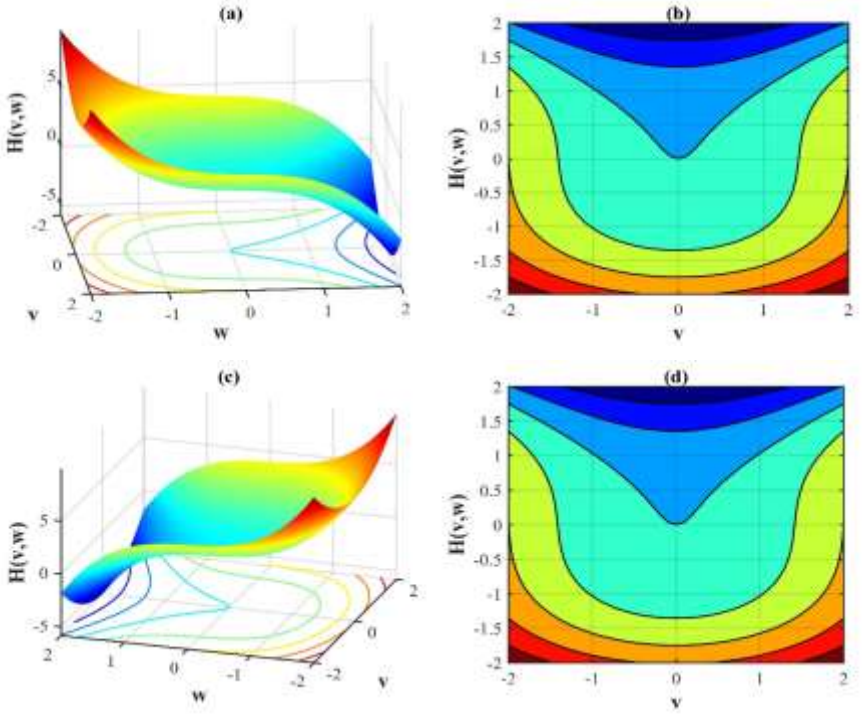

Figure 2 Geometrical structure of the model (4.2) over the range $-4 \leq v, w \leq 4$ we attain surface and contour plots.

For the values, $A = 0.5$, and $B = 0.5$, Figure 1(A) streamlines represent O-saddle point and P-center point. Conversely, Figure 1(B) streamlines show O-center point and P-saddle point. Next, we graphically illustrate the model (4.2) and also discuss the physical explanation.

Using the exact numerical values, we draw the surface plot and contour plot of the model (4.2) that we watch in Figure 2. We observed that the streamlines and surface plot gave the same results.

RESULTS AND DISCUSSIONS

In this part, we discuss the solutions attained by the research effort. This section also describes the real-life significance of the solitary waves and their physical importance. This section includes two sub-sections: The graphical representation is shown here.

Graphical representation

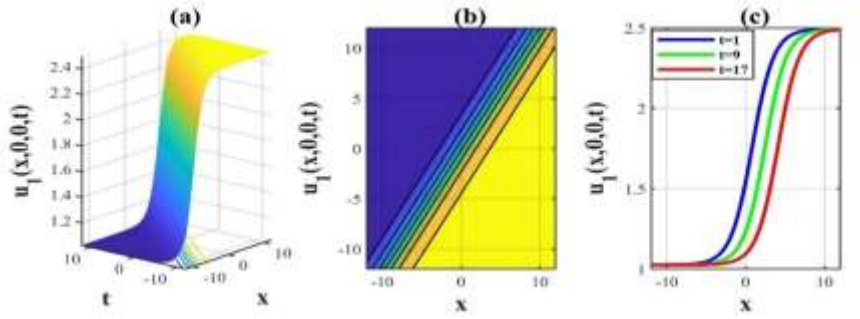

Figure 3 Anti-kink shape soliton $u_1(\xi)$ for selected parameters over the range $-12 \leq x, t \leq 12$, (a) surface, (b) contour, and (c) combined 2D graphs for distinct values of t

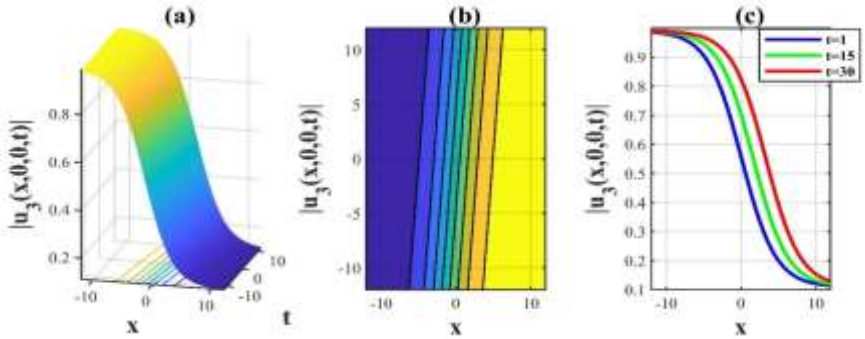

Figure 4 Kink shaped soliton $u_3(\xi)$ for selected parameters within the range $-12 \leq x, t \leq 12$ (a) surface, (b) contour, and (c) combined 2D graphs for distinct values of t

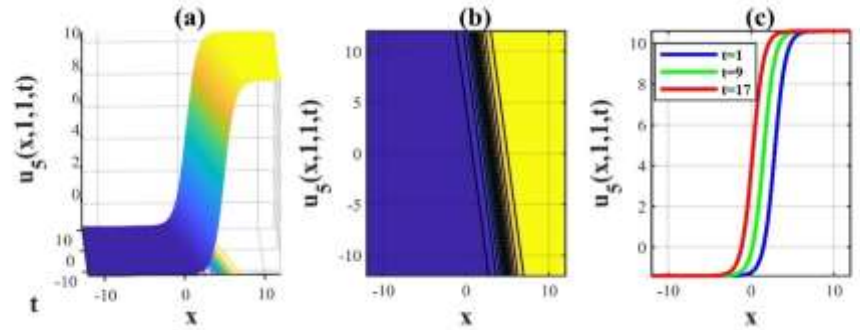

Figure 5 Anti-kink shape soliton $u_5(\xi)$ within the range $-12 \leq x, t \leq 12$ (a) surface, (b) contour, and (c) combined 2D graphs for distinct values of t

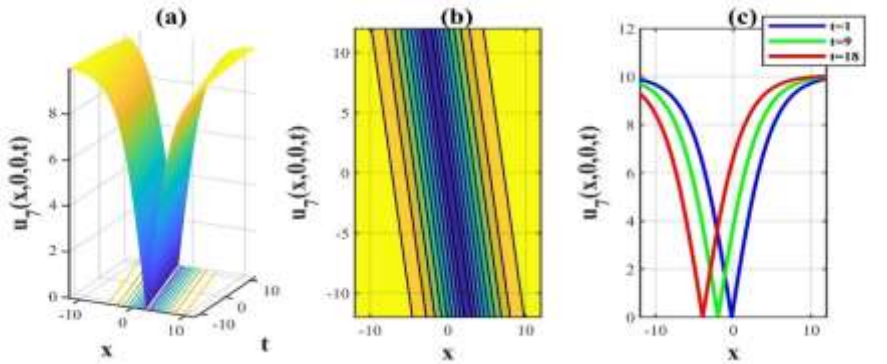

Figure 6 Dark bright or V-shaped soliton $u_7(\xi)$ over the range $-12 \leq x, t \leq 12$ (a) surface, (b) contour, and (c) combined 2D graphs for distinct values of t

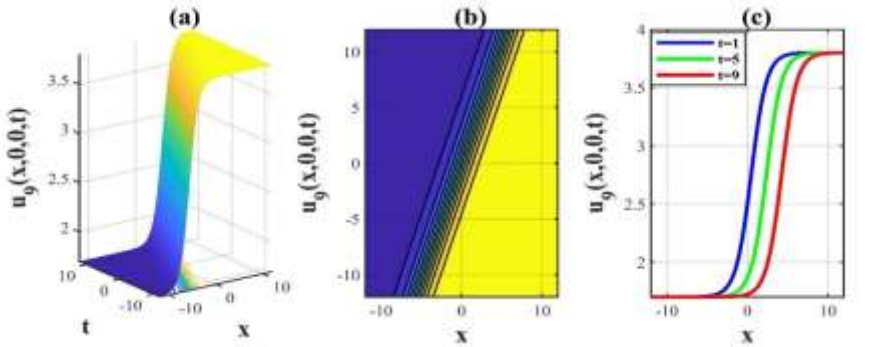

Figure 7 Anti-kink shape soliton $u_9(\xi)$ over the range $-12 \leq x, t \leq 12$ (a) surface, (b) contour, and (c) combined 2D graphs for distinct values of t

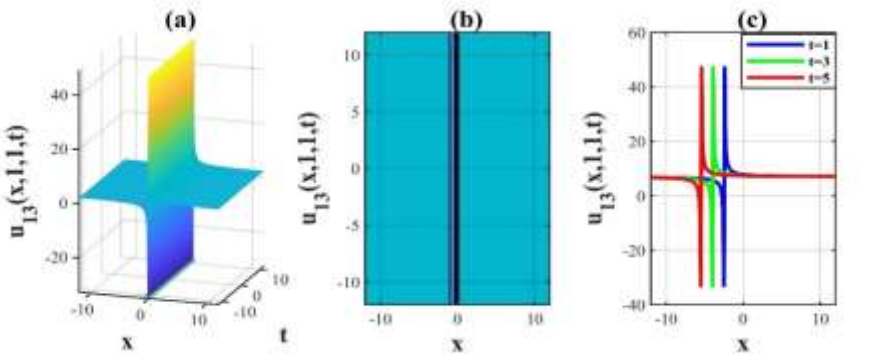

Figure 8 Singular soliton $u_{13}(\xi)$ over the range $-12 \leq x, t \leq 12$ (a) surface, (b) contour, and (c) combined 2D graphs for distinct values of t

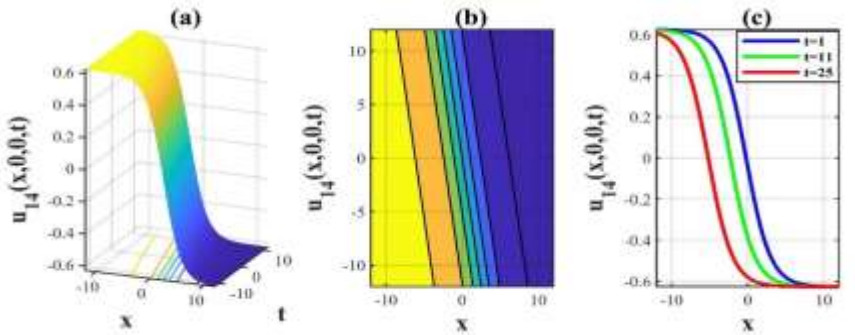

Figure 9 Kink shape soliton $u_{14}(\xi)$ within the interval $-12 \leq x, t \leq 12$ (a) surface, (b) contour, and (c) combined 2D graphs for distinct values of t

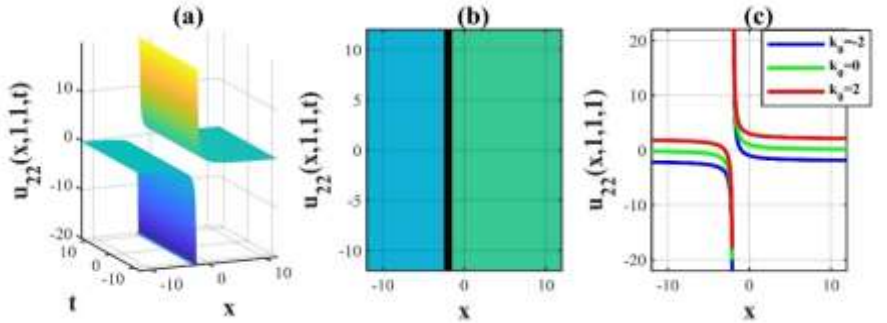

Figure 10 Singular kink shape soliton $u_{22}(\xi)$ over the range $-12 \leq x, t \leq 12$ (a) surface, (b) contour, and (c) combined 2D graphs for distinct values of k_0

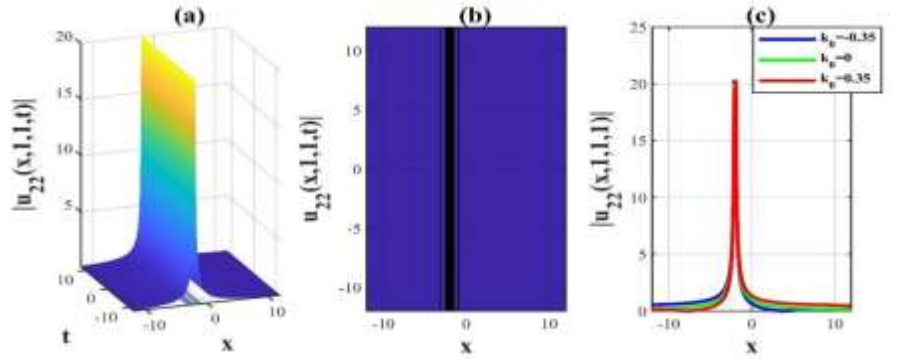

Figure 11 Singular bell-shaped soliton $u_{22}(\xi)$ is portrayed for selected parameters over the range $-12 \leq x, t \leq 12$ and we attain (a) surface, (b) contour, and (c) combined 2D graphs for distinct values of k_0

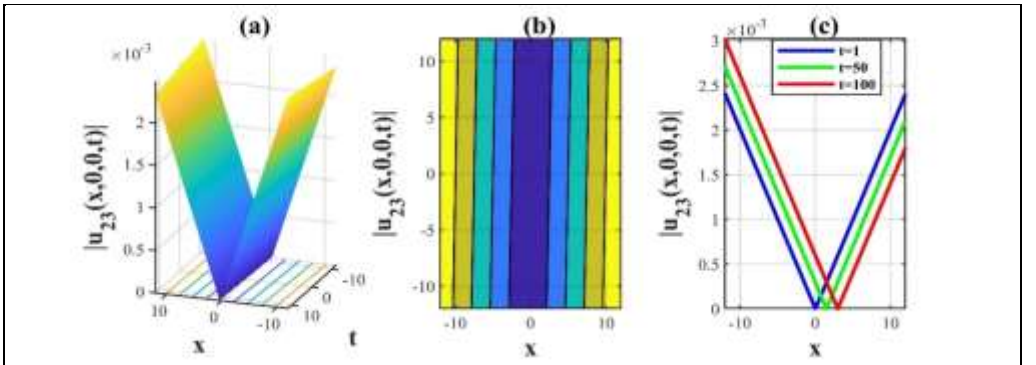

Figure 12 Flat V-shaped soliton $u_{23}(\xi)$ within the interval $-12 \le x, t \le 12$ (a) surface, (b) contour, and (c) combined 2D graphs for distinct values of t

Physical explanation

Our main goal is to demonstrate how the free parameters influence the wave profiles in the wave function $u(x, y, z, t)$ solutions to the (3+1)-dimensional JME and describe each wave's steady propagation through 3D, contour, and combination 2D plots. The solution $u_1(\xi)$ represents an anti-kink shape soliton for selecting free parametric values $p = 0.8, q = 0.5, r = -1, b = 1, c = 2.2, d = 1, y = z = k_0 = 0$ is displayed in Figure 3(a) and associated contour in Figure 3(b) in order that. Figure 3(c) also illustrates the progression of the waves for distinct values of t = 1,3,5. To increase the value of t, the graph moves horizontally forward. The modulus solution $u_3(\xi)$ represents a shaped soliton for electing free parametric values $p = 0.15, q = 2.1, r = 0.1, b = -1, c = 3, d = -1, y = z = 0, k_0 = -1$ is portrayed in Figure 4(a) and related contour in Figure 4(b) respectively. Figure 4(c) also shows the progression of the waves for different values of t = 1,15,30. To increase the value of t, the graph moves forward in a positive direction. The solution $u_5(\xi)$ layout anti-kink shape soliton for choosing free parametric values $p = 0.3, q = -0.2, r = -0.7, b = 2, c = 3, d = -2, y = z = k_0 = 1$ is as seen in Figure 5(a) and involved contour in Figure 5(b). The progression of the waves for different values of t = 1,9,17 is presented in Figure 5 (c). To increase the value of t, the diagram goes horizontally backward. The solution $u_7(\xi)$ illustrated dark bright or V-shaped soliton for determining free parametric values $p = 0.04, q = 1, r = 0.2, b = 5, c = 1, d = -5, y = z = 0, k_0 = -1$ is depicted in Figure 6(a) and similar contour in Figure 6(b) respectively. Figure 6(c) also depict the progression of the waves for different values of t = 1,9,18. The graph moves in a negative x-axis direction for increasing the value of t. The solution $u_9(\xi)$ portrayed anti-kink shape soliton for selecting free parametric values $p = 0.7, q = 0.8, r = -0.1, b = 1, c = 2.5, d = 1, y = z = 0, k_0 = 1$ is portraited in Figure 7(a) and involved contour in Figure 7(b) correspondingly. Figure 7(c) also characterizes the progression of the waves for different values of t = 1,5,9. The figure moves, simultaneously increasing the value of t in the positive x-axis direction. The solution $u_{13}(\xi)$ depicted singular soliton for picking free parametric values $p = 0.7, q = 0, r = 0.1, b = 1, c = 2, d = 1, y = z = k_0 = 1$ is demonstrated in Figure 8(a) and connected contour in Figure 8(b) in order that. Figure 8(c) illustrates the progression of the waves for different values of t = 1,3,5. To increase the value of t, the graph moves horizontally backward. The solution $u_{14}(\xi)$ illustrated kink shape soliton for selecting unrestricted parametric values $q = 0.3, p = 0.7, r = 0.5, b = 0.2, c = 0, d = -1, y = z = k_0 = 0$ is shown in Figure 9(a) and equivalent contour in Figure 9(b) respectively. Figure 9(c) also shows the progression of the waves for different values of t = 1,11,25. The figure moves in a negative x-axis direction to

increase the value of t. The solution $u_{22}(\xi)$ layout singular kink shape soliton for selecting free parametric values $q = 0.2, p = 0.1, r = 0.2, b = c = 0, d = -1, y = z = 1, k_0 = 0$ is represented in Figure 10(a) and associated contour in Figure 10(b). Figure 10(c) also shows the progression of the waves for different values of $t = -2,0,2$. To increase the value of t, the graph moves vertically upward. The modulus solution $u_{22}(\xi)$ represents a singular bell-shaped soliton for choosing free parametric values $p = 0.1, q = 0.2, r = 0, b = c = 0, d = -1, y = z = 1, k_0 = 0$ is shown in Figure 11(a) and associated contour in Figs. 11(b) in order that. Figure 11(c) also shows the progression of the waves for different values of $t = -0.35,0,0.35$. The diagram is going on vertically downward after increasing the value of t. The absolute solution $u_{23}(\xi)$ depicted a flat V-shaped soliton for picking free parametric values $p = 0.01, q = -0.1, r = 0.2, b = 1, c = 0, d = 1, y = z = k_0 = 0$ is displayed in Figure 12(a) and similar contour in Figure 12(b). Figure 12(c) also shows the progression of the waves for different values of $t = 1,50,100$. To increase the value of t, the graph moves horizontally forward.

COMPARISON

We compare our results with those of Ma & Lee (2009), who used the rational function technique to study the $(3 + 1)$-dimensional JME. Ma & Lee (2009) have found an exact solution to the stated equation by employing this method. Conversely, we applied the new auxiliary equation technique and generated abundant wave profile solutions for the $(3 + 1)$-dimensional JME. Both methods have similar solutions but are not precisely the same as displayed in Table 1. We have other solutions in the form of rational, exponential, trigonometric, and hyperbolic structures.

Table 1: Comparison between obtained solutions with rational function method solutions (Ma & Lee, 2009)

Obtained solutions	Ma & Lee (2009) solutions
In Eq.(3.5) taking $p = q = r = b = d = 1$, $c = k_0 = 0$ and $u_1(x, y, z, t) = H$, then the solution becomes $$H = -2\tan\left(x + y + z + \frac{7}{2}t\right)$$	In Eq.(3.12) taking $a = b = c = 1, d = 0$ and $u(x, y, z, t) = H$, then the solution becomes $$H = -2\tan\left(x + y + z + \frac{7}{2}t\right)$$
In Eq.(3.6) taking $p = q = r = b = d = 1$, $c = k_0 = 0$ and $u_2(x, y, z, t) = H$, then the solution becomes $$H = 2\cot\left(x + y + z + \frac{7}{2}t\right)$$	In Eq.(3.13) taking $a = b = c = 1, d = 0$ and $u(x, y, z, t) = H$, then the solution becomes $$H = 2\cot\left(x + y + z + \frac{7}{2}t\right)$$
In Eq.(3.26) taking $p = q = r = b = d = 1$, $c = 2, k_0 = 0$ and $u_{22}(x, y, z, t) = H$, then the solution becomes $$H = \frac{2}{x + y + z + \frac{3}{2}t}$$	In Eq.(3.14) taking $a = b = 1, c = \frac{1}{2}, d = 0$ and $u(x, y, z, t) = H$, then the solution becomes $$H = \frac{2}{x + y + z + \frac{3}{2}t}$$

CONCLUSION

We have successfully obtained the traveling wave solution of the $(3 + 1)$-dimensional JME by applying the new auxiliary equation technique. The traveling wave solutions produced under certain conditions can be written as rational, exponential, trigonometric, and

hyperbolic functions. However, the new auxiliary equation method provides several distinctive free parameter values, including kink, anti-kink, singular kink, dark-bright or V-shape, flat V-shaped, singular soliton, and singular bell-shaped solutions. We have mentioned 3D, contour, and combined 2D graphs to clarify the acquired solutions. We will better understand the wave velocity effect by watching the combined 2D plot. Therefore, based on the analytical investigation and the numerical solutions, we can determine that our suggested approach provides a sequential mathematical tool for studying solutions or solitary wave solutions of the (3 + 1)-dimensional JME. However, we investigated the phase plane analysis of the model. Different conditions on the involved parameters are used to find all potential phase portraits. We observe that the NAE method is simple, potent, and straightforward for handling any nonlinear model that produces abundant analytically novel soliton solutions. Shortly, we will find variable coefficient solutions of the same model to obtain more dynamics.

Funding Declaration: We do not have a research fund for this research work.

REFERENCE

Alaoui, M. K., Uddin, M., Roshid, M. M., Roshid, H. O., Osman, M. S. (2024). Modulation instability, and dynamical behavior of solitary wave solution of time M-fractional clannish random Walker's Parabolic equation via two analytic techniques. *Partial Differ. Equ. Appl.* ***12***, 101011.

Al-Ramadhani, S. (2024). On the Reduction and Solution of The Reverse Space-Time Nonlocal Fokas–Lenells Equation. *Partial Differ. Equ. Appl. 101046*.

Alshammari, F.S., Asif, M., Hoque, M.F., Aldurayhim, A. (2023). Bifurcation analysis on ion sound and Langmuir solitary waves solutions to the stochastic models with multiplicative noises. *Heliyon.* ***9(6).***

Alshammari, F.S., Roshid, H.O., Alkhorayef, A.S., Elsadany, A.A., Aldurayhim, A. (2024). Dynamics of solitary waves, chaotic behaviors, and Jacobi elliptic wave solutions in telecommunication systems. *Results Phys.* ***60,*** 107629.

Arshed, S., Akram, G., Sadaf, M., Irfan, M., Inc M. (2024). Extraction of exact soliton solutions of (2+1)-dimensional Chaffee-Infante equation using two exact integration techniques. *Opt Quantum Electron.* ***56(6),*** 1-15.

Baskonus, H.M., Bulut, H., Sulaiman, T.A. (2019). New complex hyperbolic structures to the lonngren-wave equation by using sine-gordon expansion method. *Appl. math. nonlinear sci.* ***4(1),*** 129-138.

Khater, M.M., Seadawy, A.R., Lu, D. (2018). Dispersive optical soliton solutions for higher order nonlinear Sasa-Satsuma equation in mono mode fibers via new auxiliary equation method. *Superlattices and Microstructures.* ***113,*** 346-358.

Liu, J.G., Yang, X.J., Feng, Y.Y. (2020). On integrability of the extended (3+1)-dimensional Jimbo-Miwa equation. *Math. Methods Appl. Sci.* ***43(4),*** 1646-1659.

Lü, X., Ma, W.X., Khalique, C.M. (2015). A direct bilinear Bäcklund transformation of a (2+1)-dimensional Korteweg–de Vries-like model. *Appl. Math. Lett.* ***50***, 37-42.

Ma, W.X. (2005). Complexiton solutions of the Korteweg–de Vries equation with self-consistent sources. *Chaos, Solit. Fractals,* ***26(5)***, 1453-1458.

Ma, W.X. (2022). Soliton solutions by means of Hirota bilinear forms. *Partial Differ. Equ. Appl.* ***5***, 100220.

Ma, W.X., Huang, T., Zhang, Y. (2010). A multiple exp-function method for nonlinear differential equations and its application. *Phys. scr.* ***82*****(6)**, 065003.

Ma, W.X., Lee, J.H. (2009). A transformed rational function method and exact solutions to the (3+1)-dimensional Jimbo-Miwa equation. *Chaos Solit. Fractals.* ***42*****(3),** 1356-1363.

Ma, W.X., Zhang, Y., Tang, Y., Tu, J. (2012). Hirota bilinear equations with linear subspaces of solutions. *Appl. Math. Comput.* ***218*****(13),** 7174-7183.

Ma, W.X., Zhu, Z. (2012). Solving the (3+1)-dimensional generalized KP and BKP equations by the multiple exp-function algorithm. *Appl. Math. Comput.* ***218*****(24)**, 11871-11879.

Malfliet, W. (2004). The tanh method: a tool for solving certain classes of nonlinear evolution and wave equations. *Comput. Appl. Math.* ***164*****,** 529-541.

Mehdipoor, M., Neirameh, A. (2015). New soliton solutions to the (3+1)-dimensional Jimbo-Miwa equation. *Optik.* ***126*****(23),** 4718-4722.

Mirhosseini-Alizamini, S.M., Rezazadeh, H., Srinivasa, K., Bekir, A. (2020). New closed form solutions of the new coupled Konno–Oono equation using the new extended direct algebraic method. *Pramana.* ***94*****(1),** 52.

Mirzazadeh, M., Eslami, M., Milovic, D., Biswas A. (2014). Topological solitons of resonant nonlinear Schrödinger's equation with dual-power law nonlinearity by (G'/G)-expansion technique. *Optik.* ***125*****(19),** 5480-5489.

Osman, M.S., Korkmaz, A., Rezazadeh, H., Mirzazadeh, M., Eslami, M., Zhou, Q. (2018). The unified method for conformable time fractional Schro¨dinger equation with perturbation terms. *Chin. J. Phys.* ***56*****(5),** 2500-2506.

Roshid, M.M., Ali, M.Z., Rezazadeh, H. (2020). Kinky periodic pulse and interaction of bell wave with kink pulse wave propagation in nerve fibers and wall motion in liquid crystals. *Partial Differ. Equ. Appl.* **2,** 100012.

Tuffour, F., Barnes, B., Dontwi, I. K., Darkwah, K. F. (2024). The modified homogeneous balance methods for solving Korteweg–DeVries equations. *Partial Differ. Equ. Appl. 101035*.

Ur Rehman, H., Iqbal, I., Mirzazadeh, M., Hashemi, M.S., Awan, A.U., Hassan, A.M. (2024). Optical solitons of new extended (3+1)-dimensional nonlinear Kudryashov's equation via ϕ^6-model expansion method. *Opt Quantum Electron.* ***56*****(3),** 279.

Wang, X., Bilige, S. (2020). Novel interaction phenomena of the (3+1)-dimensional Jimbo-Miwa equation. *Commun Theor Phys.* ***72*****(4),** 045001.

Wang, Y.H., Wang, H., Dong, H.H., Zhang, H.S., Temuer, C. (2018). Interaction solutions for a reduced extended (3+1)-dimensional Jimbo-Miwa equation. *Nonlinear Dyn.* ***92*****,** 487-497.

Wazwaz, A.M. (2007). Multiple-soliton solutions for the KP equation by Hirota's bilinear method and by the tanh-coth method. *Appl. Math. Comput.* ***190*****(1),** 633-640.

Wazwaz, A.M. (2017). Multiple-soliton solutions for extended (3+1)-dimensional Jimbo-Miwa equations. *Appl. Math. Lett.;* ***64*****,** 21-26.

Yue, Y., Huang, L., Chen, Y. (2019). Localized waves and interaction solutions to an extended (3+1)-dimensional Jimbo-Miwa equation. *Appl. Math. Lett.* ***89,*** 70-77.

Zhang, H., Ma, W.X. (2014). Extended transformed rational function method and applications to complexiton solutions. *Appl. Math. Comput.* ***230***, 509-515.

Zhang, R.F., Li, M.C., Yin, H.M. (2021). Rogue wave solutions and the bright and dark solitons of the (3+1)-dimensional Jimbo-Miwa equation. *Nonlinear Dyn.* ***103*****(1),** 1071-1079.

Zhang, X., Chen, Y. (2017). Rogue wave and a pair of resonance stripe solitons to a reduced (3+1)-dimensional Jimbo-Miwa equation. *Commun Nonlinear Sci Numer Simul.* ***52,*** 24-31.

Zhang, Y., Sun, S., Dong, H. (2017). Hybrid solutions of (3+1)-dimensional Jimbo-Miwa equation. *Math. Probl. Eng*. ***2017*****(1)** 5453941.

--0--